Full-metal K-Ka Dual-Band Shared-Aperture Array Antenna fed by combined Ridge-Groove Gap Waveguide

Miguel Ferrando-Rocher, *Student Member, IEEE,* Jose I. Herranz-Herruzo, *Member, IEEE,* Alejandro Valero-Nogueira, *Senior Member, IEEE,* Bernardo Bernardo-Clemente

***Abstract*—This paper presents an 8×8 dual-band shared-aperture array antenna operating in K (19.5-21.5 GHz) and Ka-band (29-31 GHz) using Gap Waveguide technology. Radiating elements consist of circular apertures located on the top plate of the antenna and excited by two stacked cavities with different diameters for dual-frequency operation. A waffle grid is used on top to increase the effective area of apertures and reduce grating lobes. Each stacked cavity is fed by its appropriate corporate-feeding network: the upper feeding layer operates at 20-GHz band and the lower one at 30-GHz band. As a result, the antenna presents two ports, one for each band, which radiate a directive farfield pattern with linear polarization, orthogonal to each other. Experimental results show impedance and radiation pattern bandwidths larger than 1.5 GHz in both bands.**

I. Introduction

Today, the integration of multiple systems has become one of the development trends in wireless technologies. Therefore, there is growing interest in shared apertures for multi-band, multi-polarized or multi-functional antennas [1]-[4]. They are attractive solutions since the number of antennas on the platform can be reduced and the aperture utilization ratio can be greatly improved. Nonetheless, this type of structures has rarely been addressed beyond the K-band and are usually based on printed solutions. The reduction in the number of antennas is especially appealing in satellite communications where high efficiency is also a must. Therefore, purely metallic structures operating at two distinct non-adjacent frequency bands are highly appreciated.

Mobile satellite terminals need to be lightweight, low-profile, and capable of tracking satellites. As a consequence of this demand, there is currently a wide interest for innovative antennas able to fullfill all or part of these needs. Planar, low-profile, lightweight, high-gain, dual-polarized and dual-band array solutions have become a popular research area over the classical solution using parabolic reflectors.

In the last decade, gap waveguide (GW) technology has proven to be a suitable candidate to develop high-gain low-profile antennas in the millimeter-wave band [5]. The fundamental principle of operation of GW relies upon two parallel plates, being one a perfect electric conductor and the other a high-impedance surface, separated less than a quarter wavelength and realized by a textured surface made of periodic metal nails. Then, a groove or a ridge embedded in such surface allows a confined field propagation along the created path. Here, a corporate feeding network combining ridges and grooves is used. This compact network provides a uniform power distribution suitable for array feeding, as successfully demonstrated in other GW array antennas in Ka-band [6]. Taking advantage of these GW features, a multitude of linearly-polarized [7], circularly-polarized [8] or dual-polarized antennas [9] have been developed already. However, the dual-band capability has not been addressed yet.

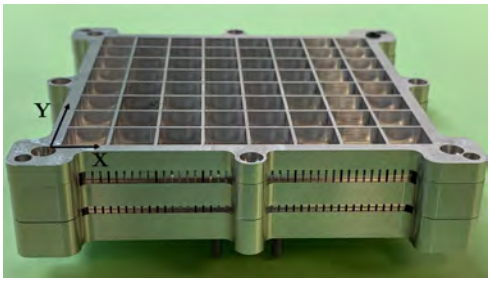

(a)

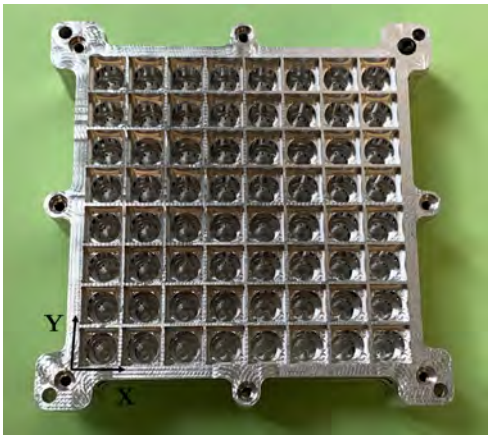

(b)

Fig. 1: Manufactured 8×8 dual-band array antenna.

In this work, we present a full-metal low-profile dual-band shared-aperture array antenna (see Fig. 1) with high gain (above 25 dBi in the lower band and close to 30 dBi in the upper band), high efficiency (above 80% in both bands), and wide impedance bandwidth (≥ 1.5 GHz in both bands too). The proposed array architecture is appropriate for satellite communication terminals, whose targeted bands are in the range of 20-GHz for receive (K-band) and 30-GHz for transmit (Ka-band).

This article has been accepted for publication in a future issue of this journal, but has not been fully edited. Content may change prior to final publication. Citation information: DOI 10.1109/LAWP.2019.2919928, IEEE Antennas and Wireless Propagation Letters

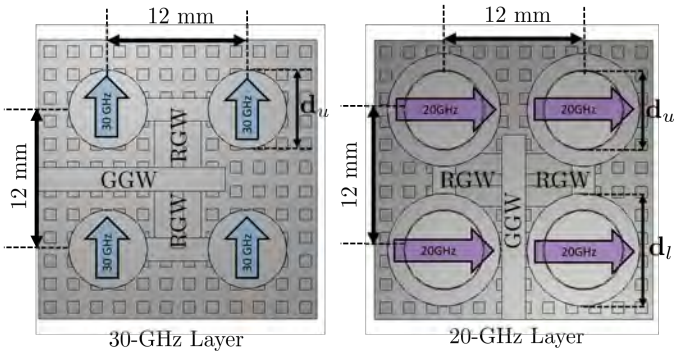

Fig. 2: Top view of the feeding layers for the basic cell (2×2 subarray).

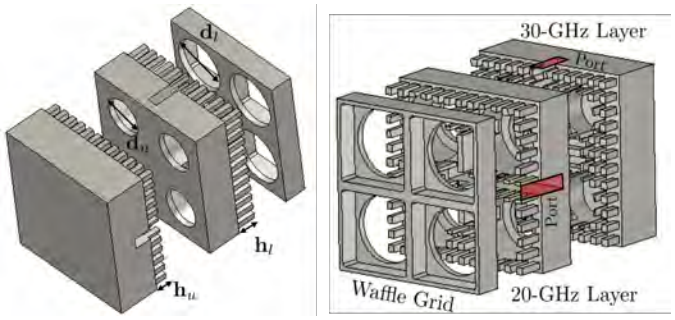

Fig. 3: Layers of the dual-band basic cell.

II. 2×2 Dual-Band Basic Cell

Figs. 2 and 3 show different views of the 2×2 dual-band unit cell. Each radiating element consists of a circular aperture, excited by two stacked cylindrical cavities, which in turn are fed from their side. For efficient radiation, the cavity radius must be λ_0/π, being λ_0 the free-space wavelength. Taking this fact into consideration, stacked cavities with different diameters are combined for a dual-band operation. Hence, the diameter of the cavity working at $f_l = 20$ GHz is d_l=9.5 mm while that operating at $f_u = 30$ GHz is d_u=6.5 mm. Obviously, the 30-GHz cavity is placed below, so that the field at 30 GHz can propagate through the cylindrical 20-GHz waveguide to finally be radiated. This architecture is inspired by the proposal in [9]. The main difference now is to use cavities with different radius to achieve the dual-band performance. Fig. 3 shows an exploded view of the stacked cylindrical cavities. It is observed that cavities at the two layers are fed at 90° from each other, hence exciting orthogonal field polarization.

Regarding the textured surface, both layers present some slight differences. The nails of the lower layer have a height of a quarter wavelength at 30 GHz (Ka-band), which is h_u=2 mm. In the upper layer, where the center frequency is around 20 GHz (K-band), the height of the nails is h_l=3.5 mm. Nail width (w_{nail}=1.4 mm) and periodicity (p_{nail}=2 mm) are identical in both layers for ease of design. The distance between apertures is 12 mm, i.e., $0.8\lambda_l$ at 20 GHz and $1.2\lambda_u$ at 30 GHz. This separation between apertures would lead to unacceptable grating lobes at 30 GHz but they are mitigated with a waffle-grid plate, as described in [8].

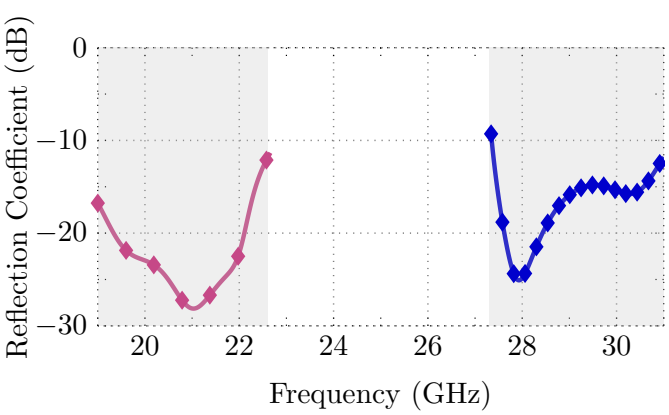

Fig. 4: Simulated reflection coefficient of the 2×2 basic cell.

A. Simulated results

The S_{11}-parameter for both ports of the 2×2 basic cell is plotted in Fig. 4. Periodic boundary conditions have been used to emulate a larger array. K-band and Ka-band operation bandwidths are clearly distinguished. The reflection coefficient at the lower band port is below −20 dB from 19.5 GHz to 22 GHz, covering beyond the bandwidth of interest. S_{11}-parameter at the upper band port is better than −15 dB from 27.5 GHz to 30.5 GHz, thus obtaining more than 10% of relative bandwidth. In Fig. 5 simulated normalized radiation patterns in XZ and YZ-planes for both bands are shown, where a 4×4 array factor has been applied. Predictably, due to the separation of $1.2\lambda_u$ at 30 GHz, grating lobes show up in both planes around $\theta = 60°$. The rest of the patterns agree with a uniform array distribution and look fairly stable in frequency. These results are experimentally confirmed below.

III. 8×8 Dual-Band Array Antenna.

The full array consists of 4×4 basic cells like the one described above. Radiating elements are fed by two 1 to 64 corporate-feed networks, one at each layer, shown highlighted in Figs. 6a and 6b. The employed architecture, already described in [10], sequentially combines Ridge (RGW) and Groove Gap Waveguides (GGW) to uniformly feed all cavities in phase. Notice also that the 90° rotation of the layers favours an improved decoupling between input ports.

Figs. 6a and 6b use a color scheme for a better reading. GGW are colored in red and RGW in green. The 30-GHz input port is colored in blue and the 20-GHz input port in yellow. Note that the 20-GHz port must cross the lower 30-GHz layer (yellow waveguide in Fig. 6a) to reach the upper layer. The different radius of the cavities in each level can also be observed in these figures. Then, above these two pieces, the top lid is placed. Two pictures of the three aluminum pieces fabricated (top and bottom view) are shown in Figs. 6c and 6d.

A. Experimental results

The experimental results of the manufactured prototype are summarized in Tables I and II and can be observed in Figs. 7, 8 and 9. The first of these figures corresponds to the S-parameters measured for each of the ports.

This article has been accepted for publication in a future issue of this journal, but has not been fully edited. Content may change prior to final publication. Citation information: DOI 10.1109/LAWP.2019.2919928, IEEE Antennas and Wireless Propagation Letters

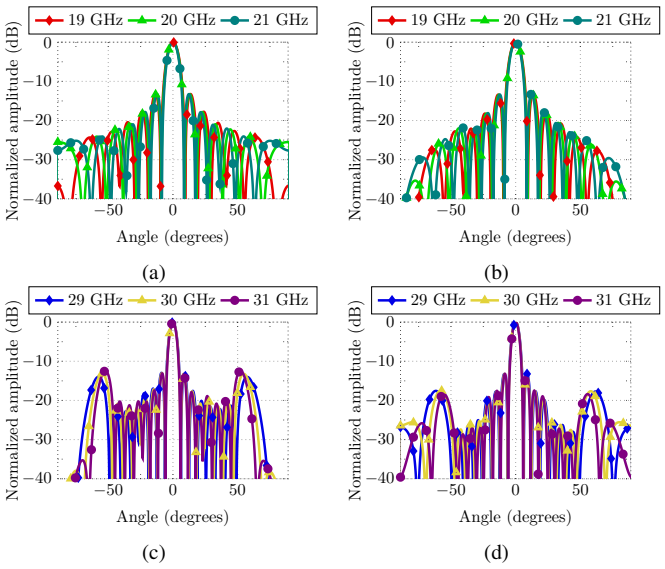

Fig. 5: Normalized simulated copolar patterns for the basic cell at several frequencies using a 4×4 array factor: K-band port in (a) XZ-plane and (b) YZ-plane; Ka-band port in (c) XZ-plane and (d) YZ-plane.

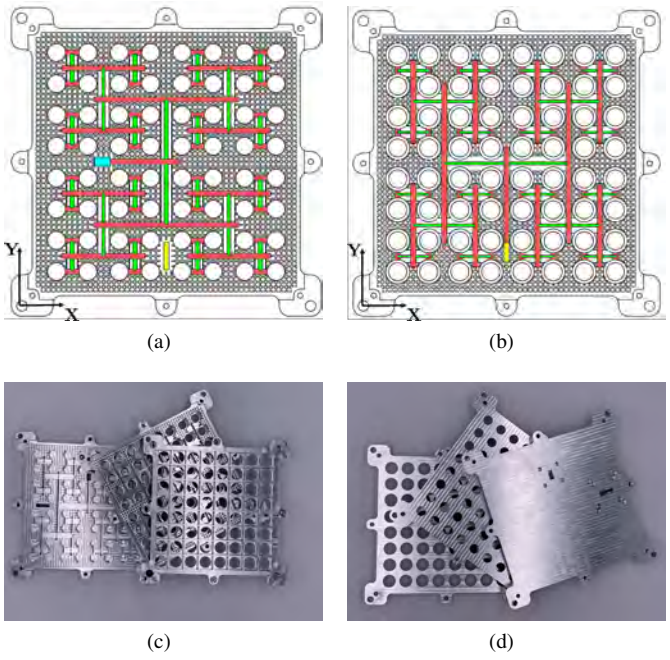

Fig. 6: (a) Top view of 30-GHz layer; (b) top view of 20-GHz layer. Photograph of the three metallic pieces comprising the manufactured dual-band antenna: (c) top view and (d) bottom view.

Reflection coefficient is below −10 dB from 19.7 to 21.5 GHz, complying broadly with the band of interest (19.7 to 21.2 GHz). Concerning the upper band, the reflection coefficient is represented from 29 GHz to 31 GHz. Even though the S_{11} does not remain below −10dB along the whole represented band, it does so from 29.7 to 31 GHz. Thus, the objective of covering the band from 29.5 a 31 GHz is close to be fulfilled.

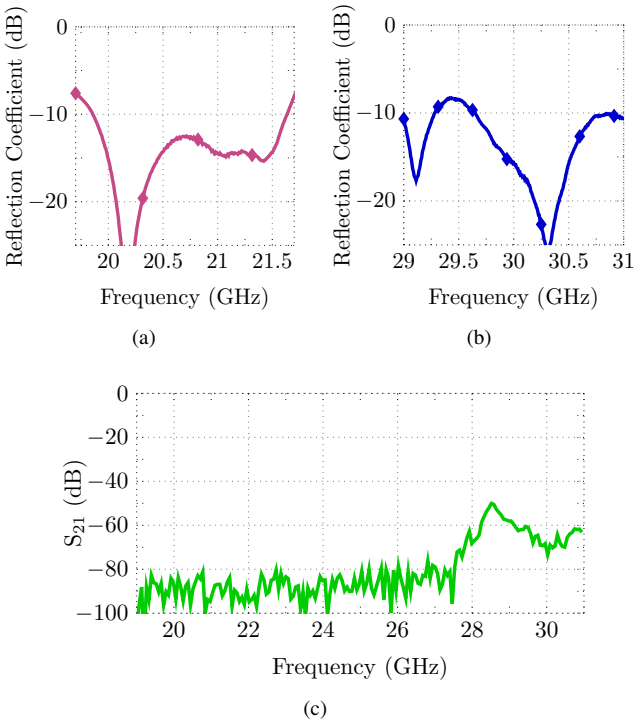

Fig. 7: Measured S-parameters: (a) S_{11} at 20-GHz port, (b) S_{11} at 30-GHz port and (c) S_{21}.

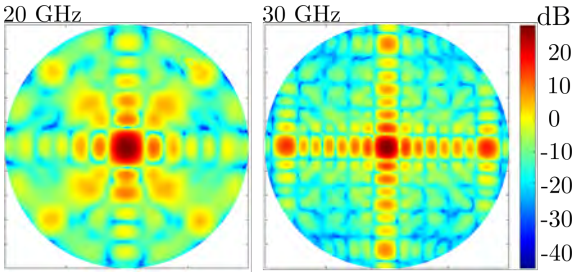

Fig. 8: 2D Measured radiation pattern at 20 GHz (left) and 30 GHz (right).

With reference to the radiation patterns, 2D representations are displayed in Fig. 8 for each center frequency (20 GHz and 30 GHz). Fig. 8 is obtained from an in-house tool that determines the spherical-field modal decomposition. These modes are later used to calculate the far-field at any point [11].

Besides, in Fig 9 the main cuts are shown at various frequencies in each band: from 19 to 21.5 GHz and from 29 to 31 GHz. The results are highly satisfactory, very similar to those obtained in simulation. Grating lobes appearing at the upper band, mostly in the XZ-plane, were predicted by simulations. Their maximum level, however, do not surpass the secondary lobe level and may be considered as acceptable.

The measurement data displayed in Tables I and II reveal an antenna efficiency above 80% in both bands, being the maximum gain 26 dBi and 29.5 dBi in the lower and upper bands, respectively.

Finally, Table III shows a performance comparison between proposed and reported dual-band antennas implemented with

This article has been accepted for publication in a future issue of this journal, but has not been fully edited. Content may change prior to final publication. Citation information: DOI 10.1109/LAWP.2019.2919928, IEEE Antennas and Wireless Propagation Letters

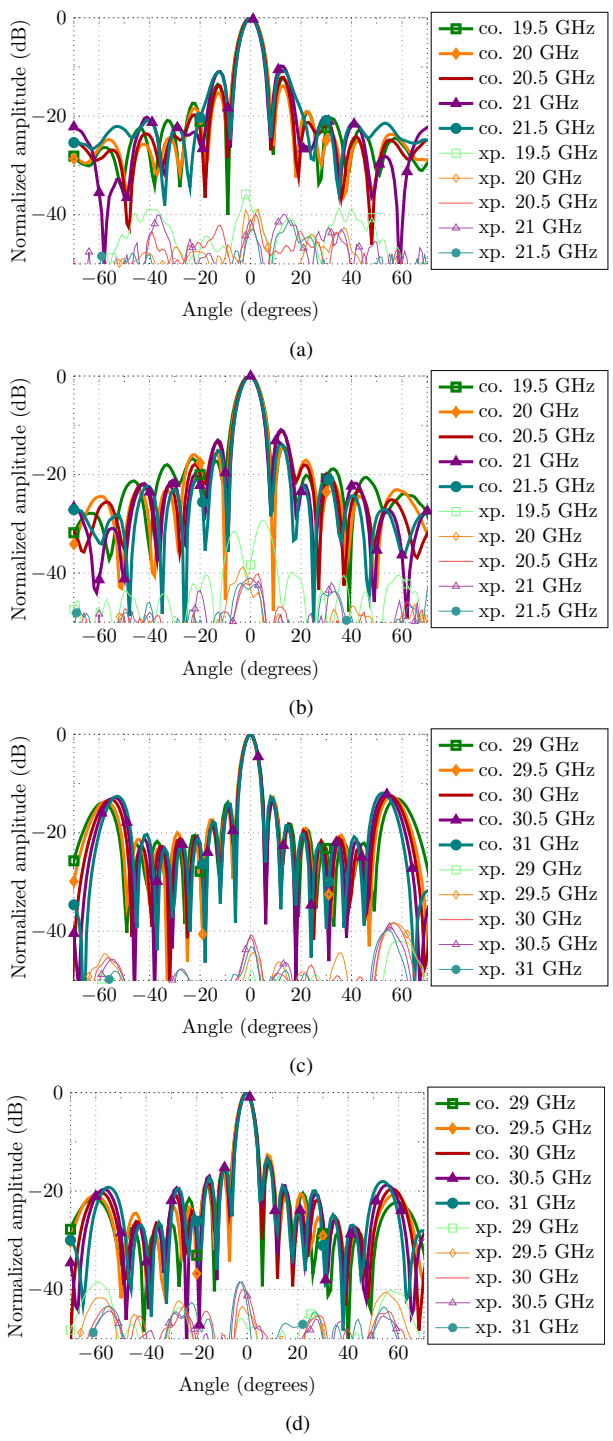

Fig. 9: Normalized copolar and crosspolar measured radiation patterns for several frequencies: K-band port in (a) XZ-plane and in (b) YZ-plane; Ka-band port in (c) XZ-plane and in (d) YZ-plane.

different technologies.

IV. Conclusions

An 8×8 dual-band antenna array using Gap Waveguide technology, mainly intended for satellite communications, is presented. The radiating elements consist of shared circular apertures excited by stacked cylindrical cavities, fed in turn by two feeding layers operating at K and Ka-band. This proof of concept proposes for the first time a full-metal GW antenna with two non-adjacent working bands. Experimental results demonstrate that the proposed scalable array architecture provides the desired dual-band performance as well as a high efficiency and good radiation and impedance bandwidth.

Grating lobes presence due to the larger array spacing at the upper band might be mitigated by several approaches, e.g. by using a frequency selective surface on a superstrate. It should be also noted that the grating lobes level would certainly decrease for other FDD systems with closer bands. Both this issue and the fact of achieving circular polarization are not minor and should be faced to comply with the strict system requirements.

TABLE I: Measured antenna parameters at K-band.

Frequency (GHz)	19.5	20.0	20.5	21.0	21.5
Directivity (dBi)	25.71	26.15	26.72	26.75	26.64
Gain (dBi)	24.68	25.40	25.86	25.85	26.03
Antenna Efficiency (%)	78.88	84.14	82.04	81.28	86.90

TABLE II: Measured antenna parameters at Ka-band.

Frequency (GHz)	29.0	29.5	30.0	30.5	31.0
Directivity (dBi)	29.55	29.56	29.83	29.87	29.98
Gain (dBi)	28.48	29.00	29.30	29.04	29.49
Antenna Efficiency (%)	78.15	88.03	88.44	82.58	89.42

TABLE III: Performance comparison between proposed and reported dual-band array antennas.

Reference	This Work	[4]	[12]	[13]
Bands	K—Ka	K—Ka	L—Ka	Ku-Ka
BW (%)	10—6	n/a	4—3	16—5
Max. Gain (dBi)	26—29.5	24—27	9—29	28—28
Mean Eff. (%)	83—85	n/a	n/a—60	n/a
Technology	GW	Transmitarray	μstrip	Reflectarray
Full Metal	Yes	No	No	No

V. Acknowledgements

This work has been supported by the Spanish Ministry of Economy and Competitiveness (Ministerio de Economía y Competitividad) under the project TEC2016-79700-C2-1-R.

References

[1] Y. R. Ding and Y. J. Cheng, "Ku/ka dual-band dual-polarized shared-aperture beam scanning antenna array with high isolation," *IEEE Transactions on Antennas and Propagation*, 2019.

[2] J. F. Zhang, Y. J. Cheng, Y. R. Ding, and C. X. Bai, "A dual-band shared-aperture antenna with large frequency ratio, high aperture reuse efficiency and high channel isolation," *IEEE Transactions on Antennas and Propagation*, 2018.

[3] F. Qin, S. S. Gao, Q. Luo, C.-X. Mao, C. Gu, G. Wei, J. Xu, J. Li, C. Wu, K. Zheng *et al.*, "A simple low-cost shared-aperture dual-band dual-polarized high-gain antenna for synthetic aperture radars," *IEEE Transactions on Antennas and Propagation*, vol. 64, no. 7, pp. 2914–2922, 2016.

[4] S. A. Matos, E. B. Lima, J. S. Silva, J. R. Costa, C. A. Fernandes, N. J. Fonseca, and J. R. Mosig, "High gain dual-band beam-steering transmit array for satcom terminals at ka-band," *IEEE Transactions on Antennas and Propagation*, vol. 65, no. 7, pp. 3528–3539, 2017.

[5] P.-S. Kildal, E. Alfonso, A. Valero-Nogueira, and E. Rajo-Iglesias, "Local metamaterial-based waveguides in gaps between parallel metal plates," *IEEE Antennas and Wireless Propagation Letters*, vol. 8, pp. 84–87, 2009.

[6] M. Ferrando-Rocher, J. I. Herranz-Herruzo, A. Valero-Nogueira, and B. Bernardo-Clemente, "Performance assessment of gap-waveguide array antennas: Cnc milling versus three-dimensional printing," *IEEE Antennas and Wireless Propagation Letters*, vol. 17, no. 11, pp. 2056–2060, 2018.

[7] A. J. Sáez, A. Valero-Nogueira, J. I. Herranz, and B. Bernardo, "Single-layer cavity-backed slot array fed by groove gap waveguide," *IEEE Antennas and Wireless Propagation Letters*, vol. 15, pp. 1402–1405, 2016.

[8] M. Ferrando-Rocher, J. I. Herranz-Herruzo, A. Valero-Nogueira, and A. Vila-Jiménez, "Single-layer circularly-polarized ka-band antenna using gap waveguide technology," *IEEE Transactions on Antennas and Propagation*, vol. 66, no. 8, pp. 3837–3845, 2018.

[9] M. Ferrando-Rocher, J. I. Herranz-Herruzo, A. Valero-Nogueira, B. Bernardo-Clemente, A. Zaman, and J. Yang, "8×8 ka-band dual-polarized array antenna based on gap waveguide technology," *Accepted for publication: IEEE Transactions on Antennas and Propagation*, vol. 67, no. 7, pp. 1–10, 2019.

[10] M. Ferrando-Rocher, A. Valero-Nogueira, and J. I. Herranz-Herruzo, "New feeding network topologies for high-gain single-layer slot array antennas using gap waveguide concept," in *Antennas and Propagation (EUCAP), 2017 11th European Conference on*. IEEE, 2017, pp. 1654–1657.

[11] J. Hald and F. Jensen, *Spherical near-field antenna measurements*. Iet, 1988, vol. 26.

[12] I. Russo, C. Canestri, A. Manna, G. Mazzi, and A. Tafuto, "Dual-band antenna array with superdirective elements for short-distance ballistic tracking," *IEEE Transactions on Antennas and Propagation*, vol. 67, no. 1, pp. 232–241, 2019.

[13] E. Martinez-de Rioja, J. A. Encinar, M. Barba, R. Florencio, R. R. Boix, and V. Losada, "Dual polarized reflectarray transmit antenna for operation in ku-and ka-bands with independent feeds," *IEEE Transactions on Antennas and Propagation*, vol. 65, no. 6, pp. 3241–3246, 2017.